HOSTED BY
ELSEVIER
CrossMark
Available online at www.sciencedirect.com
ScienceDirect
Defence Technology 12 (2016) 101–105
www.elsevier.com/locate/dt

Numerical simulation of interior ballistic process of railgun based on the multi-field coupled model

Qing-hua LIN *, Bao-ming LI
National Key Laboratory of Transient Physics, Nanjing University of Science & Technology, Nanjing 210094, China

Received 30 September 2015; revised 23 December 2015; accepted 24 December 2015
Available online 6 February 2016

Abstract

Railgun launcher design relies on appropriate models. A multi-field coupled model of railgun launcher was presented in this paper. The 3D transient multi-field was composed of electromagnetic field, thermal field and structural field. The magnetic diffusion equations were solved by a finite-element boundary-element coupling method. The thermal diffusion equations and structural equations were solved by a finite element method. A coupled calculation was achieved by the transfer data from the electromagnetic field to the thermal and structural fields. Some characteristics of railgun shot, such as velocity skin effect, melt-wave erosion and magnetic sawing, which are generated under the condition of large-current and high-speed sliding electrical contact, were demonstrated by numerical simulation.

Keywords: Railgun; Electromagnetic field; Thermal field; Structural field; Finite element; Numerical simulation

1. Introduction

The application of electromagnetic force in defense technology is receiving more and more attention [1]. Research on the interior ballistics of railgun requires the detailed analysis of launch components, such as armature and rail, which exhibit the coupled electromagnetic, thermal and structural behaviors. The accurate numerical simulation and modeling of electromagnetic process are crucial to treat the multi-field coupled problem. But some features of a railgun launcher make it difficult to model: the railgun launcher is inherently three-dimensional, and the high-speed sliding electric contact between rail and armature is involved during a railgun shot. Some computer programs, such as EMAP3D [2], MEGA [3] and HERB [4], were developed to simulate the electromagnetic diffusion process under the condition of high-speed sliding electric contact. Recently, an electromagnetism module was added to the LS-DYNA dynamics analysis software [5] for the coupled mechanical/thermal/electromagnetic simulations.

Besides the electromagnetic field analysis, the thermal and structural aspects are becoming even more important at the weapon level currents conducted in rails and armature. Many potentially interesting features, such as structural deformation and armature melting, can be obtained more easily from numerical simulation than from experiment.

The models, algorithms and results of the multi-field analyses for railgun were presented in the paper. The electromagnetic and thermal equations were solved by an in-house program code. The simulated results of electromagnetic field were transferred as forcing functions to the structural module of LS-DYNA, and the structural dynamic responses of a railgun were obtained.

2. Theoretical model and numerical method

2.1. Basic assumptions

The load transfer methods were used to couple the electromagnetic, thermal and structural fields. The results of electromagnetic analysis were transferred to the thermal and structural analyses. In order to facilitate the multi-field computation, the following assumptions were made: (a) only metallic components, such as armature and rail, were considered in a model; (b) the nonlinear properties of materials were ignored; (c) the contact surface between armature and rail was smooth; (d) one-way coupling was used, and the calculation of the electromagnetic field provided ohmic heating power loads for thermal conduction and Lorentz force loads for structural field.

Peer review under responsibility of China Ordnance Society.
* Corresponding author. Tel.: +86 2584315938 821.
E-mail address: tsh_lin@sina.com (Q.H. LIN).

http://dx.doi.org/10.1016/j.dt.2015.12.008
2214-9147/

2.2. Magnetic diffusion equations

The electromagnetic field was modeled by magnetic diffusion equations in the Lagrange coordinate system. Using the magnetic vector potential $\vec{A}$ and electric scalar potential ϕ as unknown quantities, a set of magnetic diffusion equations, which can be deduced from quasi-static Maxwell's equations, is expressed as

$$\begin{cases} \nabla\times\dfrac{1}{\mu}\nabla\times\vec{A}=\sigma\left(-\dfrac{\mathrm{D}\vec{A}}{Dt}-\nabla\phi\right) \\ \nabla\cdot\left[\sigma\left(-\dfrac{\mathrm{D}\vec{A}}{\mathrm{D}t}-\nabla\phi\right)\right]=0 \end{cases} \tag{1}$$

where μ is the permeability of conductors and σ is the electrical conductivity. For non-conductive regions, the Laplace equation can be deduced form Eq. (1) due to negligible electrical conductivity.

A hybrid finite element and boundary element coupling algorithm was used in the calculation of the magnetic diffusion equations [6]. The finite-element formulation based on the Galerkin form of weighted residuals method was used for the magnetic diffusion equations for the conductive region including rail and armature. The discretized magnetic equations are approximated by the following matrix form as

$$\left(\mathbf{K}+\frac{\mathbf{M}}{\Delta t}\right)\cdot[\mathbf{A}]^{n+1}=\frac{\mathbf{M}}{\Delta t}\cdot[\mathbf{A}]^{n}-\mathbf{P}\cdot[\varphi]^{n+1}+\mathbf{S}\cdot\left[\frac{\partial\mathbf{A}}{\partial n}\right]^{n+1} \tag{2}$$

where **K**, **M**, **P** and **S** are the coordinate matrices. For the non-conductive region, the boundary element formulation was used for Laplace's equation. The boundary integral equation was discretized into matrix form as follows

$$\mathbf{H}[\mathbf{A}]^{n+1}=\mathbf{G}\left[\frac{\partial\mathbf{A}}{\partial n}\right]^{n+1} \tag{3}$$

where **H** and **G** are the influence matrices. After a left multiplication of $\mathbf{SG}^{-1}$, Eq. (3) is added to Eq. (2), yielding the following set of equations

$$\left(\mathbf{K}+\frac{\mathbf{M}}{\Delta t}+\mathbf{SG}^{-1}\mathbf{H}\right)\cdot[\mathbf{A}]^{n+1}=\frac{\mathbf{M}}{\Delta t}\cdot[\mathbf{A}]^{n}-\mathbf{P}\cdot[\varphi]^{n+1} \tag{4}$$

2.3. Thermal diffusion equation

Under the assumption of energy balance, a 3D form of the thermal diffusion equation was deduced in a moving coordinate system

$$\rho c\frac{\mathrm{D}T}{\mathrm{D}t}-\nabla\cdot(\kappa\nabla T)=\dot{Q} \tag{5}$$

where T, ρ, c and κ are temperature, solid density, specific heat and thermal conductivity, respectively; and $\dot{Q}$ is the heat load generated in the conductor due to ohmic heating. $\dot{Q}$ can be expressed as

$$\dot{Q}=\frac{\vec{J}\cdot\vec{J}}{\sigma} \tag{6}$$

where $\vec{J}$ is the current density which can be expressed by

$$\vec{J}=-\sigma\left(\frac{\mathrm{D}\vec{A}}{\mathrm{D}t}+\nabla\phi\right) \tag{7}$$

In the temperature field calculation, a sparse symmetric matrix was generated by a finite element method based on the Galerkin form of weighted residuals.

2.4. Structural equation

Only the elastic processes of the armature and rails were considered to facilitate the coupling calculation. The governing equations based on conservation of momentum are expressed in the form of tensor as

$$s_{ij,j}+f_i=\rho\ddot{u}_i \tag{8}$$

where s, f and u are stress tensor, force per unit volume and structural displacement, respectively. The Galerkin method was used to discretize the structural equations to the finite element formulas which are expressed as follows

$$\mathbf{M}\left\{\frac{\mathrm{d}^2\mathbf{u}}{\mathrm{d}t}\right\}+\mathbf{K}\cdot\{\mathbf{u}\}=\{\mathbf{F}(t)\} \tag{9}$$

where **M** and **K** are mass matrix and stiffness matrix, respectively; and **F** is force vector that can be obtained from electromagnetic field. The time-dependent Lorentz force density is described as

$$\vec{F}=\vec{J}\times\vec{B} \tag{10}$$

where $\vec{B}$ is the magnetic flux density which can be expressed as

$$\vec{B}=\nabla\times\vec{A} \tag{11}$$

2.5. Numerical method

The electromagnetic and thermal fields were expressed by diffusion equations. The computational domain was discretized using the Galerkin method, and the time derivative terms were approximated by a backward difference scheme which is unconditionally stable. Same integration time step was chosen for solving the electromagnetic and thermal equations. The linear algebraic equations of the electromagnetic and thermal fields were solved by a preconditioned generalized conjugate residual (GCR) method [7] and an incomplete Cholesky conjugate gradient (ICCG) method [8], respectively.

The structural field was described by the dynamic equations with second-order derivative terms of the time. Due to the flexibility of LS-DYNA in explicit dynamics calculation and its extensive application in ballistics research [9], LS-DYNA was used as a solver for the structural equations. Although the characteristic time scale of structural field are quite different from that of other physical fields, the time step was controlled automatically in LS-DYNA.

The node variables were transferred among the different physical fields by using a same mesh of 8-node hexahedron solid elements for solving the electromagnetic, thermal and structural equations.

3. Results and discussion

A 3D transient analysis of a solid-armature railgun was examined. The mesh of coupled multi-field model including armature and rails is shown in Fig. 1. The unit of geometric size in Fig. 1 is millimeter. The initial conductor temperature was set to 25 °C.

Table 1 lists the material properties used in calculation. The symbols σ, ρ, E, ν, c and κ represent electrical conductivity, density, modulus of elasticity, Poisson's ratio, heat capacity and thermal conductivity, respectively.

Pulsed current was applied on the breech segment of railgun model. The armature was accelerated by the Lorentz force, which is generated by the action of current and magnetic fields. The profiles of the imposed current and armature velocity are shown in Fig. 2. The armature velocity reached 2623 m/s.

3.1. Results of electromagnetic field analysis

The contours of current density distribution during a railgun shot are shown in Fig. 3. A current diffusion process was demonstrated by the current density gradient at different times. Higher current density appeared on some edges of rail and armature. As the armature is accelerated to a higher speed, a high current density gradient arises and the velocity skin effect (VSE) occurs in the local areas of the rails which are passed by the armature. VSE [10] is an electrodynamic phenomenon that causes the current to concentrate on the edges of moving conductors.

In addition to the current density, some other physical parameters can be obtained by Eqs. (6), (7), (10) and (11). In Figs. 4–7, the vector of current density, vector of magnetic flux

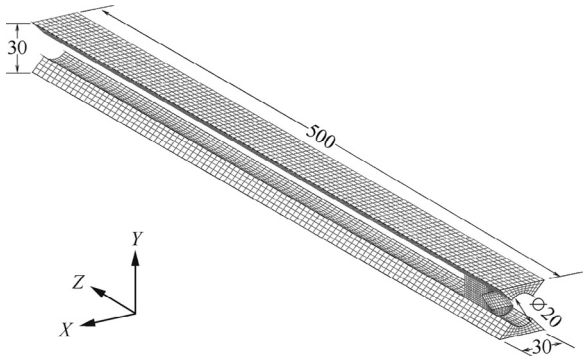

Fig. 1. Mesh of multi-field model for a round bore railgun.

Table 1
Material properties used in calculation.

	σ/(S·m^{-1})	ρ/(kg·m^3)	E/Pa	ν	c/J/(kg·K)	κ/W/(m·K)
Rail	4.6×10^7	8.9×10^3	1.3×10^{11}	0.30	385	397
Armature	1.9×10^7	2.8×10^3	7.2×10^{10}	0.33	960	130

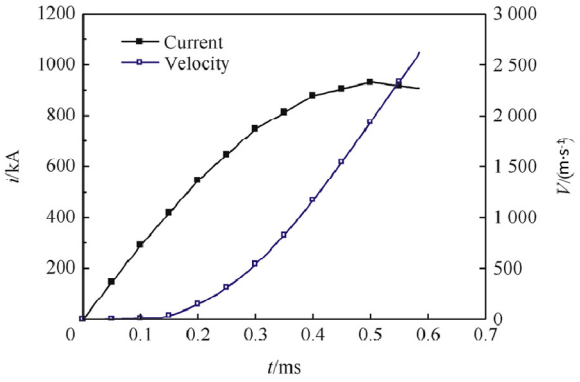

Fig. 2. Profiles of imposed current and armature velocity.

density, contour of ohmic heating power density and vector of Lorentz force are demonstrated, respectively.

3.2. Results of thermal field analysis

The predicted results of ohmic heating power obtained from magnetic diffusion calculations were transferred to the thermal field, and the evolution of temperature distribution on the rail and armature was obtained. The armature was always in a current-carrying state during a shot, so the rise of temperature on the armature is more obvious than that on the rail. The contours of the armature temperature distribution are shown in Fig. 8.

Temperature rise leads to the melting of the armature. It can be seen from Fig. 8 that the melting regions are present mainly

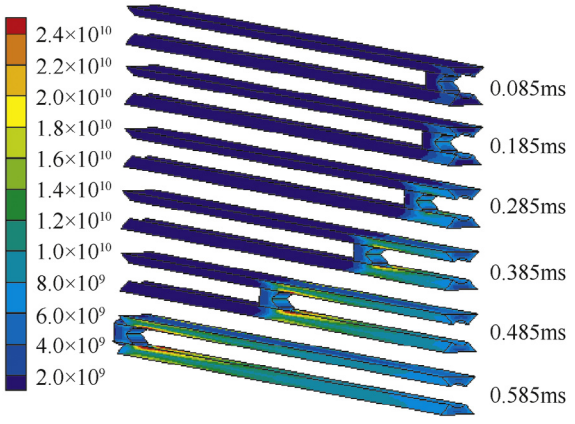

Fig. 3. Evolution of current density at different time steps (A/m^2).

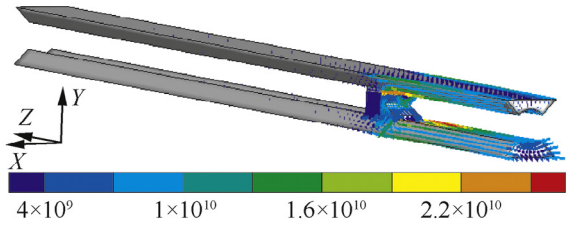

Fig. 4. Vector of current density at 0.385 ms (A/m^2).

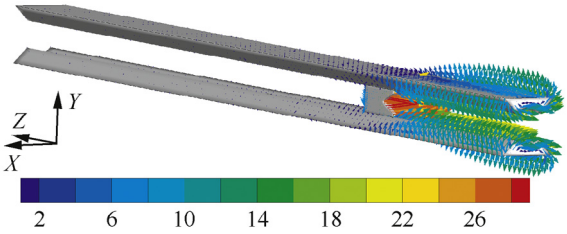

Fig. 5. Vector of magnetic flux density at 0.385 ms (Tesla).

at the armature throat and on the sliding contact surface. Melting starts from the trailing edge of the armature. This phenomenon is melt-wave erosion (MWE) [11] and is caused by the velocity skin effect of which the current clusters at the rear of armature arms.

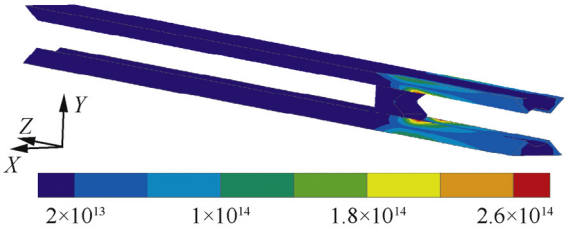

Fig. 6. Contour of ohmic heating power density at 0.385 ms (W/m^3).

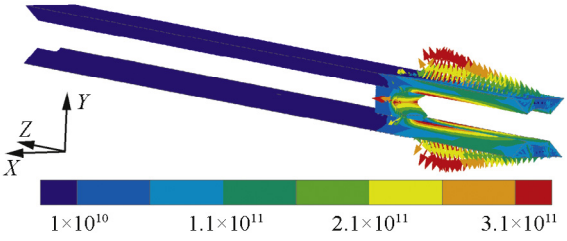

Fig. 7. Vector of Lorentz force at 0.385 ms (N/m^3).

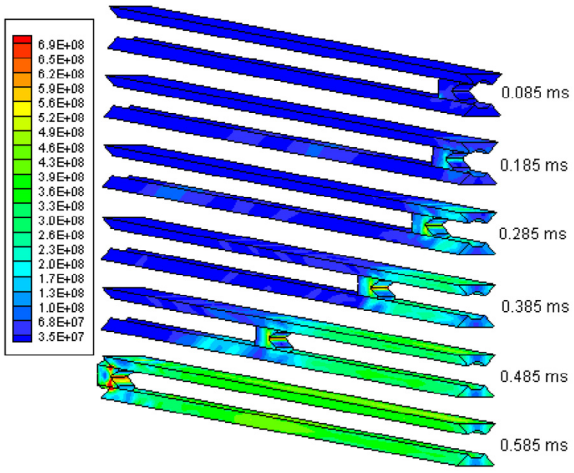

Fig. 9. Contour of Von Mises stress in the rails (Pa).

3.3. Results of structural field analysis

The Lorentz force generated by the current and electromagnetic fields was applied for the calculation of structural field. Fig. 9 shows the Von Mises stress distribution at different time steps. The dynamic response of the rail structure during railgun shot is given in Fig. 9.

It can be seen from Figs. 8 and 9 that the maximum stress and high temperature simultaneously appear at the throat of the armature. Potential damage, which is called magnetic sawing [12], is prone to occur at the throat.

4. Summary

The railgun problem is a multi-field coupled problem, for which not only an electromagnetic field should be analyzed in detail, but also the thermal and structural fields should be analyzed simultaneously to determine the dynamics of rail and armature. In this paper, the coupling calculation was achieved by the load transfer among electromagnetic, thermal and structural fields. Some typical phenomena in railgun, such as current diffusion, velocity skin effect, melt-wave erosion and magnetic sawing, were demonstrated by numerical simulation. The results indicate that the models and algorithms in this paper are feasible to treat the railgun multi-field problem.

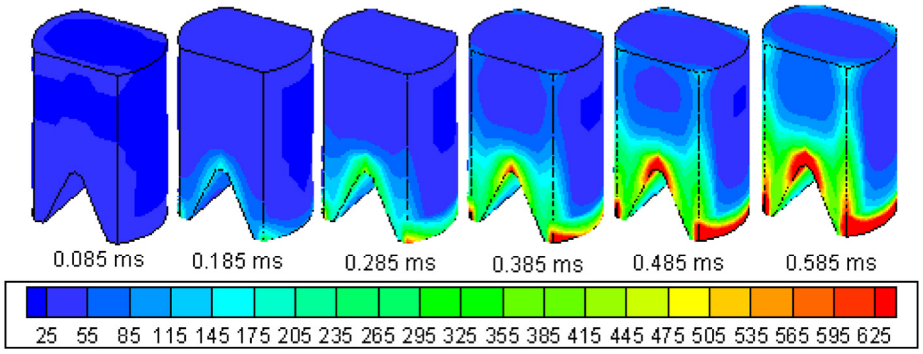

Fig. 8. Evolution of armature temperature (°C).

References

[1] Zhang H, Fan B, Chen Z, Li H, Li B. Experimental research on the mechanism of lift amplification and vibration suppression of Lorentz force. Def Technol 2013;9(2):85–90.

[2] Hsieh K-T, Kim B. Implementing tri-potential approach in EMAP3D. IEEE Trans Magn 1999;35(1):166–9.

[3] Rodger D, Lai HC. A comparison of formulations for 3D finite element modeling of electromagnetic launchers. IEEE Trans Magn 2001; 37(1):135–8.

[4] Shatoff H, Pearson DA, Kull AE. Simulation of dynamic armature motion in a railgun with coupling of electromagnetic, thermal and structural effects using shifted finite element fields. Presented at the 15th International Pulsed Power Conference, May 25–28, 2005.

[5] Caldichoury I, L'Eplattnier P. Simulation of a railgun: a contribution to the validation of the electromagnetism module in LS-DYNA ®v980. Presented at the 12th International LS-DYNA® Users Conference, 2012.

[6] Lin QH, Li BM, Kwok DY. Transient heating effects in electromagnetic launchers with complex geometries: a 3D hybrid FE/BE analysis. Eur Phys J Spec Top 2009;171:135–43.

[7] Xu S. Theory and method of matrix computation. Beijing: Peking University Press; 1995. p. 183–7.

[8] Xie D, Yang S. Numerical analysis and synthesis of engineering electromagnetic field. Beijing: China Machine Press; 2009. p. 224–33.

[9] Zhao H, Xie J, Li Z, Zhang H. Experiment and simulation of launching process of a small-diameter steel cartridge case. Def Technol 2014; 10(4):349–53.

[10] Cowan M. Solid-armature railguns without the velocity-skin effect. IEEE Trans Magn 1993;29(1):385–90.

[11] Stefani F, Merrill R. Experiments to measure melt-wave erosion in railgun armatures. IEEE Trans Magn 2003;39(1):188–92.

[12] Melton D, Watt T, Crawford M. A study of magnetic sawing in an aluminum bar. IEEE Trans Magn 2007;43(1):170–2.